Dynamical study of T_{ss} systems using the chiral quark model*

Jiazheng Ji (纪家正)† Yuheng Xing (邢玉恒)‡ Xinxing Wu (吴新星)§ Ning Xu (徐宁)♮ Yue Tan (谭悦)♯

Department of Physics, Yancheng Institute of Technology, Yancheng 224051, China

Abstract: Since the discovery of T_{cc} by LHCb, there has been considerable interest in T_{cc} and its heavy-flavor partners. However, the study of its strange partner T_{ss} has been largely overlooked. Within the framework of the chiral quark model, we conducted a systematic study of the bound states of T_{ss} based on the Gaussian Expansion Method. We considered all physical channels with 01^+, including molecular and diquark structures. Moreover, by considering the coupling between diquarks and molecular states, our calculations allowed us to identify a deep bound state with a bounding energy of 60 MeV primarily composed of KK^*. Using the $^3P_0$ model, we calculated the decay width of K^* within the KK^* bound state, which is approximated as the decay width of the bound state in the T_{ss} system. These results indicate that, owing to the effect of binding energy, the decay width of K^* in KK^* is approximately 3 MeV smaller than that of K^* in vacuum. Additionally, resonance state calculations were performed. We used the real-scaling method to search for possible resonance states in the T_{ss} sysytem. Because of the strong attraction in the $[K^*]_8[K^*]_8$ configuration, four resonance states were found in the vicinity of 2.2−2.8 GeV, predominantly featuring hidden-color structures. The decay widths of these states are less than 10 MeV. We strongly recommend experimental efforts to search for the resonance states in the T_{ss} system predicted by our calculations.

Keywords: quark model, T_{ss} system, bound state, resonances

DOI: 10.1088/1674-1137/ad7c28 **CSTR:** 32044.14.ChinesePhysicsC.49013101

I. INTRODUCTION

In 1964, Gell-Mann [1] and Zweig [2] proposed the conventional quark model, suggesting that mesons and baryons are composed of $q\bar{q}$ and qqq, respectively. At that time, most hadrons were properly explained by this model. However, over the past two decades, there has been an influx of new experimental data unveiling properties of hadronic states that challenge the predictions of the conventional quark model, such as $X(3872)$ [3], $Y(4626)$ [4], and $Z_c(3900)$ [5]. These exotic hadronic states provide a valuable platform for a deeper understanding of the properties of low-lying Quantum Chromodynamics (QCD).

In 2021, the LHCb Collaboration reported a new state $T_{cc}^+(3875)$ in the $D^0D^0\pi$ mass distribution with a mass $M = 3875.1 + \delta m_{\rm exp}$, where $\delta m_{\rm exp} = -273 \pm 61 \pm 5^{+11}_{-14}$ keV, and a width $\Gamma = 410 \pm 165 \pm 43^{+18}_{-38}$ keV [6, 7]. This notably narrow width indicates that it is a long-living exotic state. Its spin-parity quantum number is $J^P = 1^+$. The minimal quark content of $T_{cc}^+(3875)$ is $cc\bar{u}\bar{d}$, which means that, unlike the three hidden-charm tetraquark states mentioned above, there can be no annihilation for such a component. These interesting properties have attracted theoretical attention and motivated research globally [8−48]. It is generally assumed that T_{cc}^+ is a molecular state, a compact tetraquark, or a triangle singularity. For example, in Ref. [8], by using a coupled-channel approach, the authors suggested that T_{cc}^+ is a hadronic molecule generated by the interactions in the $D^{*+}D^0$ and $D^{*0}D^+$ channels. In Ref. [9], they also argued that T_{cc}^+ is a molecule state in the framework of chiral unitary theory. Moreover, S. S. Agaev *et al.* [10] proposed that T_{cc}^+ is a compact structure by employing the QCD three-point sum rule method. In Refs. [11, 12], the authors proposed that this state may be a triangle logarithmic singularity.

In addition to the T_{cc} state, double-bottom (T_{bb}) tetraquark states have also been investigated in various theoretical frameworks. In Ref. [13], also using a coupled-channel approach, the authors proposed that $\bar{B}^*\bar{B}^*$ states

Received 14 June 2024; Accepted 18 September 2024; Published online 19 September 2024

* Supported partly by the National Natural Science Foundation of China (12205249) and the Funding for School-Level Research Projects of Yancheng Institute of Technology (xjr2022039, xjr2022040, xjr2020038)

† E-mail: 3078203935@qq.com

‡ E-mail: phyxyh@ycit.edu.cn

§ E-mail: wuxinxing@ycit.edu.cn

♮ E-mail: xuning79530@126.com

♯ E-mail: tanyue@ycit.edu.cn

with $IJ^P = 01^+, 11^+$ might be good molecular candidates. In Ref. [14], J. Cheng *et al.* employed a heavy diquark-antidiquark symmetry (HDAS) and the chromomagnetic interaction (CMI) model to study $bb\bar{n}\bar{n}$ ($n = u, d$) tetraquark states. The results show that the lowest energy of $bb\bar{n}\bar{n}$ with $IJ^P = 01^+$ is approximately 116 MeV below the $\bar{B}\bar{B}^*$ threshold. In Ref. [15], Lin *et al.* investigated the P-wave $T_{\bar{b}\bar{b}}$ states in the diquark-antidiquark framework by employing the quark model. In the ρ-mode with 1^1P_1 $[bb]^0_3[\bar{u}\bar{d}]^0_3$ configuration, its energy is approximately 18 MeV lower than the $\bar{B}\bar{B}$ threshold, which means it can establish a compact bound state.

Furthermore, theoretical investigations have explored other partners (T_{bc}, $T_{bc\bar{s}}$, $T_{cc\bar{s}}$, $T_{bb\bar{s}}$) of T_{cc}. In the case ofT_{bc}, $T_{bc\bar{s}}$ states, in Ref. [18] the authors employed a nonrelativistic quark model and found that T_{bc} with $IJ^P = 00^+$ and 01^+, T_{bcs} with $\frac{1}{2}0^+$, $\frac{1}{2}1^+$ can form a bound state. The high-spin states T_{bc} with 02^+ and $T_{bc\bar{s}}$ with $\frac{1}{2}2^+$ can decay into D-wave $\bar{B}D$ and $\bar{B}_sD$, although they are below the $\bar{B}^*D^*$ and $\bar{B}^*_sD^*$ thresholds, respectively. The QCD sum rule has also been used to calculate T_{bc} and T_{bc} [16, 17]. In Ref. [16], the authors suggested that for the $T_{bc\bar{s}}$ states with $J^P = 0^+$ and 1^+, both masses are below the corresponding thresholds ($D^{(*)}\bar{B}^{(*)}$). In Ref. [17], the results show that the masses of $T_{bc\bar{s}}$ tetraquark states are below the thresholds of $\bar{B}_sD$ and $\bar{B}^*_sD$ final states for the scalar and axial-vector channels, respectively. Regarding $T_{cc\bar{s}}$ and $T_{bb\bar{s}}$ tetraquark states, in Ref. [18], the authors argued that $T_{cc\bar{s}}$ is not a bound state, but they obtained a shallow bound state for the $T_{bb\bar{s}}$ tetraquark state with $IJ^P = \frac{1}{2}1^+$. Applying the color-Coulomb potential in the diquark-antidiquark framework at the heavy quark limit [19], the $T_{bb\bar{s}}$ state becomes bound into compact structures. However, in Ref. [20], the authors reported that $T_{cc\bar{s}}$ can establish a stable state against the strong interaction. Further results and discussions on the partners of T_{cc} can be found in Refs. [49−59].

While T_{cc} partners involving heavy quarks have been extensively studied, limited attention has been given to double strangeness partner (T_{ss}) tetraquark states. Thus, the investigation of bound and resonant states in the T_{ss} system is both interesting and necessary.

The structure of the paper is as follows. Section II provides a brief description of the quark model and wave functions. Section III introduces the real-scaling method. Section IV details the $^3P_0$ method. Section V presents our results and discussion.

II. CHIRAL QUARK MODEL, WAVE FUNCTION OF THE T_{ss} SYSTEM

A. Chiral quark model

In this study, we primarily investigated the dynamics of the $s\bar{q}s\bar{q}$ system using the chiral quark model. This model is an excellent potential framework because it effectively explains hadron interactions, including mass, kinetic, and potential terms, which can be expressed as

$$H = 2(m_s + m_q) + 2\left(\frac{\vec{p}^2_{s\bar{q}}}{2\mu_{s\bar{q}}}\right) + \frac{\vec{p}^2_{s\bar{q}s\bar{q}}}{2\mu_{s\bar{q}s\bar{q}}} + V(r_{ij}), \tag{1}$$

where m denotes the quark mass, μ represents the reduced mass, and $\vec{p}$ is the relative momentum between quarks. The form of μ is

$$\mu_{s\bar{q}} = \frac{m_s m_{\bar{q}}}{m_s + m_{\bar{q}}}, \quad \mu_{s\bar{q}s\bar{q}} = \frac{(m_s + m_{\bar{q}})}{2}. \tag{2}$$

In the $s\bar{q}s\bar{q}$ system, s and q can be approximately regarded as identical quarks. Consequently, the exchange of Goldstone bosons between s and q plays a significant role. Therefore, our potential includes the confinement potential, one-gluon exchange potential, and Goldstone boson exchange potential, expressed as follows:

$$V(r_{ij}) = \sum_{i<j=1}^{n}[V_{con}(r_{ij}) + V_{oge}(r_{ij}) + \sum_{\chi=\pi,\eta,K} V_\chi(r_{ij}) + V_\sigma(r_{ij})] \tag{3}$$

Goldstone boson exchange mainly stems from the spontaneous chiral symmetry breaking, a fundamental characteristic of QCD. This results in a long-range attractive force between quarks. In our chiral quark model, the chiral part of the Hamiltonian, $(V_\pi(r_{ij})+V_\eta(r_{ij})+ V_K(r_{ij})+ V_\sigma(r_{ij}))$, can be expressed as

$$\begin{aligned}
V_\pi(r_{ij}) &= \frac{g^2_{ch}}{4\pi}\frac{m^2_\pi}{12m_im_j}\frac{\Lambda^2_\pi}{\Lambda^2_\pi - m^2_\pi}m_\pi[Y(m_\pi r_{ij}) \\
&\quad - \frac{\Lambda^3_\pi}{m^3_\pi}Y(\Lambda_\pi r_{ij})]\boldsymbol{\sigma}_i\cdot\boldsymbol{\sigma}_j\sum_{a=1}^{3}\lambda^a_i\lambda^a_j, \\
V_K(r_{ij}) &= \frac{g^2_{ch}}{4\pi}\frac{m^2_K}{12m_im_j}\frac{\Lambda^2_K}{\Lambda^2_K - m^2_K}m_K[Y(m_K r_{ij}) \\
&\quad - \frac{\Lambda^3_K}{m^3_K}Y(\Lambda_K r_{ij})]\boldsymbol{\sigma}_i\cdot\boldsymbol{\sigma}_j\sum_{a=1}^{3}\lambda^a_i\lambda^a_j, \\
V_\eta(r_{ij}) &= \frac{g^2_{ch}}{4\pi}\frac{m^2_\eta}{12m_im_j}\frac{\Lambda^2_\eta}{\Lambda^2_\eta - m^2_\eta}m_\eta[Y(m_\eta r_{ij}) \\
&\quad - \frac{\Lambda^3_\eta}{m^3_\eta}Y(\Lambda_\eta r_{ij})]\boldsymbol{\sigma}_i\cdot\boldsymbol{\sigma}_j[\lambda^8_i\lambda^8_j\cos\theta_P - \sin\theta_P], \\
V_\sigma(r_{ij}) &= -\frac{g^2_{ch}}{4\pi}\frac{\Lambda^2_\sigma}{\Lambda^2_\sigma - m^2_\sigma}m_\sigma[Y(m_\sigma r_{ij}) - \frac{\Lambda_\sigma}{m_\sigma}Y(\Lambda_\sigma r_{ij})],
\end{aligned} \tag{4}$$

where $\boldsymbol{\sigma}$ represents the Pauli matrices acting on the spin

wave functions of the T_{ss} system, and λ^a denotes the Gell-Mann matrices acting on the flavor wave functions of the T_{ss} system. $Y(x)$ is the Yukawa function, explicitly given by $Y(x) = e^{-x}/x$. Λ_χ serves as the cut-off parameter, and $g_{ch}^2/4\pi$ denotes the Goldstone-quark coupling constant. The masses of Goldstone bosons are denoted by m_π, m_η, and m_K, while m_σ is determined by the relation

$$m_\sigma^2 \approx m_\pi^2 + 4m_{u,d}^2. \tag{5}$$

One of the characteristics of QCD is quark confinement, which suggests that quarks cannot be separated. This corresponds to the confinement potential in the Hamiltonian. Unlike other potential forms in the quark model, the confinement potential is not directly derived from the field theory. Consequently, it typically appears in three common forms: linear [60], quadratic [61], and screened[62] confinement potentials. These potentials share the common feature of exhibiting strong attraction at short distances. The distinction lies in the fact that, owing to screening effects, screened confinement potential can describe well the spectra of light mesons including excited states. Given that the $s\bar{q}s\bar{q}$ system involves light mesons (K/K^*), we employed the screened confinement potential in this study. Its specific form is expressed as

$$V_{\rm con}(r_{ij}) = [-a_c(1-{\rm e}^{-\mu_c r_{ij}}) + \Delta]\boldsymbol{\lambda}_i^c \cdot \boldsymbol{\lambda}_j^c, \tag{6}$$

where λ^c denotes $SU(3)$ color Gell-Mann matrices, and a_c and μ_c are model parameters.

The one-gluon exchange potential $V_{\rm oge}(r_{ij})$ reflects the QCD characteristic of asymptotic freedom. It plays a crucial role in the quark model by offering intermediate-range attractive forces. This potential generally consists of a Coulomb term and a color-magnetic term. It reads

$$V_{\rm oge}(r_{ij}) = \frac{\alpha_s}{4}\boldsymbol{\lambda}_i^c \cdot \boldsymbol{\lambda}_j^c \left[\frac{1}{r_{ij}} - \frac{1}{6m_i m_j}\boldsymbol{\sigma}_i \cdot \boldsymbol{\sigma}_j \frac{{\rm e}^{-r_{ij}/r_0(\mu_{ij})}}{r_{ij} r_0^2(\mu_{ij})}\right], \tag{7}$$

where α_s is the QCD-inspired strong coupling constant, which is determined by fitting experimental meson data. Generally, the heavier the quark, the smaller the coupling constant between quarks. All the parameters are determined by fitting the meson spectrum, from light to heavy, taking into account only a quark-antiquark component. They are listed in Table 1.

Table 1. Quark model parameters ($m_\pi = 0.7$ fm^{-1}, $m_\sigma = 3.42$ fm^{-1}, $m_\eta = 2.77$ fm^{-1}, $m_K = 2.51$ fm^{-1}).

Quark masses	$m_u = m_d$(MeV)	313
	m_s(MeV)	555
Goldstone bosons	$\Lambda_\pi = \Lambda_\sigma$(fm^{-1})	4.2
	$\Lambda_\eta = \Lambda_K$(fm^{-1})	5.2
	$g_{ch}^2/(4\pi)$	0.54
	θ_p(°)	–15
Confinement	a_c (MeV)	430
	$\mu_c(fm^{-1})$	0.7
	Δ(MeV)	181.1
OGE	α_{qq}	0.54
	α_{qs}	0.48
	α_{ss}	0.42
	$\hat{r}_0$(MeV)	28.17

B. Wave function of the T_{ss} system

The T_{ss} system has two important structures: the molecular ($s\bar{q}$-$s\bar{q}$) and diquark (ss-$\bar{q}\bar{q}$) configurations. At the quark level, these are expressed as the product of four components: color, spin, flavor, and orbital parts. According to QCD, any quark system, including multi-quark states, must be colorless. Therefore, the color wave function of a four-quark system can be obtained by two coupled color-singlet clusters, $\mathbf{1}\otimes\mathbf{1}$,

$$C_1 = \sqrt{\frac{1}{3}}(\bar{r}r + \bar{g}g + \bar{b}b) \times \sqrt{\frac{1}{3}}(\bar{r}r + \bar{g}g + \bar{b}b). \tag{8}$$

Additionally, the color wave function of a colorless four-quark system can also be obtained by coupling two color-octet wave functions, $\mathbf{8}\otimes\mathbf{8}$,

$$\begin{aligned} C_2 = \sqrt{\frac{1}{72}}(&3\bar{b}r\bar{r}b + 3\bar{g}r\bar{r}g + 3\bar{b}g\bar{g}b + 3\bar{g}b\bar{b}g + 3\bar{r}g\bar{g}r \\ &+ 3\bar{r}b\bar{b}r + 2\bar{r}r\bar{r}r + 2\bar{g}g\bar{g}g + 2\bar{b}b\bar{b}b - \bar{r}r\bar{g}g \\ &- \bar{g}g\bar{r}r - \bar{b}b\bar{g}g - \bar{b}b\bar{r}r - \bar{g}g\bar{b}b - \bar{r}r\bar{b}b). \end{aligned} \tag{9}$$

These two color wave functions correspond to the molecular configurations. Regarding the diquark structure, the color wave functions are constructed in a similar manner to the coupling of two color-octet states into a color-singlet four-quark wave function. Specifically, it involves coupling $\mathbf{3}\otimes\bar{\mathbf{3}}$ and $\mathbf{6}\otimes\bar{\mathbf{6}}$ to form a colorless four-quark system. The wave function can be expressed as

$$\begin{aligned} C_3 = \sqrt{\frac{1}{12}}(&rg\bar{r}\bar{g} - rg\bar{g}\bar{r} + gr\bar{g}\bar{r} - gr\bar{r}\bar{g} + rb\bar{r}\bar{b} \\ &- rb\bar{b}\bar{r} + br\bar{b}\bar{r} - br\bar{r}\bar{b} + gb\bar{g}\bar{b} - gb\bar{b}\bar{g} + bg\bar{b}\bar{g} - bg\bar{g}\bar{b}), \\ C_4 = \sqrt{\frac{1}{24}}(&2rr\bar{r}\bar{r} + 2gg\bar{g}\bar{g} + 2bb\bar{b}\bar{b} + rg\bar{r}\bar{g} + rg\bar{g}\bar{r} \\ &+ gr\bar{g}\bar{r} + gr\bar{r}\bar{g} + rb\bar{r}\bar{b} + rb\bar{b}\bar{r} + br\bar{b}\bar{r} \\ &+ br\bar{r}\bar{b} + gb\bar{g}\bar{b} + gb\bar{b}\bar{g} + bg\bar{b}\bar{g} + bg\bar{g}\bar{b}). \end{aligned} \tag{10}$$

In contrast to color wave functions, the spin of antiquarks and quarks is indistinguishable. Therefore, diquark and molecular structures share the same spin wave function. Given that we are studying the T_{ss} system with total spin 1, its wave function exists in three possible configurations, namely $\mathbf{0}\otimes\mathbf{1}$ (S_1), $\mathbf{1}\otimes\mathbf{0}$ (S_2), and $\mathbf{1}\otimes\mathbf{1}$ (S_3),

$$S_1=\chi^{\sigma}_{00}\chi^{\sigma}_{11}, \qquad S_2=\chi^{\sigma}_{11}\chi^{\sigma}_{00},$$
$$S_3=\frac{1}{\sqrt{2}}(\chi^{\sigma}_{11}\chi^{\sigma}_{10}-\chi^{\sigma}_{10}\chi^{\sigma}_{11}).$$

The flavor wave functions of the sub-clusters for the two structures are

$$\chi^{fm}_{\frac{1}{2},\frac{1}{2}}=s\bar{d},\chi^{fm}_{\frac{1}{2},-\frac{1}{2}}=-s\bar{u}, \tag{11}$$

$$\chi^{fd_1}_{0,0}=ss,\chi^{fd_2}_{0,0}=\frac{1}{\sqrt{2}}(\bar{u}\bar{d}-\bar{d}\bar{u}). \tag{12}$$

In this case, the subscripts of $\chi^{fm(d)i}_{I,I_z}$ denote the isospin and its third component, while the superscripts specify the structure (*fm* for the molecular configuration and *fd* for the diquark configuration) and the index. Considering the isospin of T_{cc}, the isospin of T_{ss} is set to zero. Thus, the total flavor wave function can be coupled in two possible ways: $\frac{1}{2}\otimes\frac{1}{2}$ (molecular configuration, F_1) and $\mathbf{0}\otimes\mathbf{0}$ (diquark configuration, F_2). The total flavor wave functions can be written as

$$F_1=\frac{1}{\sqrt{2}}\left(\chi^{fm}_{\frac{1}{2}\frac{1}{2}}\chi^{fm}_{\frac{1}{2}-\frac{1}{2}}-\chi^{fm}_{\frac{1}{2}-\frac{1}{2}}\chi^{fm}_{\frac{1}{2}\frac{1}{2}}\right),$$
$$F_2=\chi^{fm}_{\frac{1}{2}\frac{1}{2}}\chi^{fm}_{\frac{1}{2}\frac{1}{2}}. \tag{13}$$

Given that the T_{ss} system has positive parity, we set all orbital quantum numbers to zero. Consequently, its spatial wave function can be represented as

$$\psi(r)=\Psi_{l_1=0}(\mathbf{r}_{12})\Psi_{l_2=0}(\mathbf{r}_{34})\Psi_{L_r=0}(\mathbf{r}_{1234}).$$

The spatial wave functions for the three relative motions involved here are expanded using the Gaussian Expansion Method (GEM):

$$\Psi_{l_1=0}(r_{12})=\sum_{n1=1}^{n1_{\max}}c_{n1}N_{n1}\mathrm{e}^{-\nu_{n1}r^2}Y_{00}(\hat{r_{12}}), \tag{14}$$

$$\Psi_{l_2=0}(r_{34})=\sum_{n2=1}^{n2_{\max}}c_{n2}N_{n2}\mathrm{e}^{-\nu_{n2}r^2}Y_{00}(\hat{r_{34}}), \tag{15}$$

$$\Psi_{L_r=0}(r_{1234})=\sum_{n3=1}^{n3_{\max}}c_{n3}N_{n3}\mathrm{e}^{-\nu_{n3}r^2}Y_{00}(\hat{r_{1234}}), \tag{16}$$

with normalization constant

$$N_n=\left[\frac{4(2\nu_n)^{3/2}}{\sqrt{\pi}}\right]^{1/2}. \tag{17}$$

The coefficients c_n are variational parameters determined through dynamic optimization. The Gaussian size parameters follow a geometric progression,

$$\nu_n=\frac{1}{r_n^2}, \quad r_n=r_1a^{n-1}, \quad a=\left(\frac{r_{n_{\max}}}{r_1}\right)^{\frac{1}{n_{\max}-1}}. \tag{18}$$

Here, r_n denotes the Gaussian size parameter for the n-th term, with r_1 and $r_{n_{\max}}$ as the initial parameters.

The total wave function is constructed as the direct product of the orbital, spin, color, and flavor wave functions. Thus, the complete wave function of the system is expressed as

$$\Psi^{i,j,k}=\mathcal{A}\psi(r)S_iF_jC_k. \tag{19}$$

Here, $\mathcal{A}$ denotes the antisymmetrization operator. For the $s\bar{q}s\bar{q}$ system, where the two subsystems are identical, $\mathcal{A}$ is defined as 1-(13)-(24)+(13)(24). Subsequently, to determine the eigen-energies of the system utilizing the Rayleigh-Ritz variational principle, we solve the Schrödinger equation:

$$H\Psi^{i,j,k}=E\Psi^{i,j,k}. \tag{20}$$

III. REAL-SCALING METHOD

The real-scaling method was first proposed by Taylor [63] to study resonance states in electron-molecule systems. Owing to its success in explaining a substantial amount of experimental data, Hiyama *et al.* [64] applied this method at the quark level to search for the P_c states in the $qqqc\bar{c}$ system. Subsequently, we introduced this method to the tetraquark system for the first time and successfully explained particles [65−69] such as $Y(4626)$, $X(2900)$, and $\Upsilon(10753)$.

The real-scaling method involves systematically scaling the width of Gaussian functions between two groups using a scaling factor denoted as α, $R\to\alpha R$. As α increases, the width of the Gaussian functions expands, leading to variations in the system energy. If a stable structure is present, it remains unaffected by the changes in Gaussian function widths. Within the framework of

this method, bound states do not exhibit decay behavior owing to the absence of corresponding decay channels, and thus manifest as horizontal lines, as shown in Fig. 1(a). Conversely, resonance states, which have several decay channels, strongly couple with scattering channels and decay to the relevant threshold channels. This is depicted in Fig. 1(b) by two downward-sloping lines that demonstrate avoid-crossing behavior. Given that resonance states are stable structures, the avoid-crossing structure may reappear as the scaling factorα increases. However, a larger α results in a more complex calculation process. Therefore, for computational efficiency, we setα to range from 1.0 to 3.0. Within this range, most resonance states exhibit repeated avoid-crossing structures. The real-scaling method allows for the calculation of the decay width of stable states. The calculation equation is

$$\Gamma = 4|V(\alpha_c)|\frac{\sqrt{|Slope_r||Slope_s|}}{|Slope_r - Slope_s|}. \tag{21}$$

Based on the discussion above, in the framework of the real-scaling method, the avoid-crossing structure represents a resonant state, while the horizontal line indicates a bound state. Therefore, the decay width calculation given by Eq. (21) is applicable only to the decay width of resonant states. Here, α_c denotes the α coordinate corresponding to the avoid-crossing structure, while $V(\alpha_c)$ represents the energy difference at the avoid-crossing point between the two lines; "$slope_r$" and "$slope_s$" indicate the slopes of these two lines.

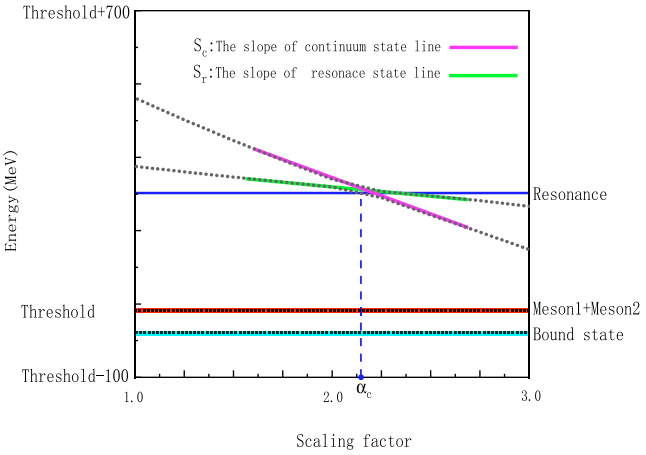

Fig. 1. (color online) Two forms of stable states, namely bound state (horizontal line) and resonance state (avoid-crossing structure), for the real-scaling method. The red line represents the threshold, while the light blue line indicates the bound state. The avoid-crossing structure formed by the red line represents the scattering state, whereas the green line represents a genuine resonance.

IV. $^3P_0$ MODEL

The $^3P_0$ model is extensively employed in the calculation of meson decay widths [70, 71]. It posits that a meson in the vacuum excites a pair of quark-antiquark with momenta $\mathbf{p}_3$ and $\mathbf{p}_4$, respectively. The probability of their production is determined by a parameter γ, which is generally determined by an overall fitting of the strong decay width of hadrons. Thus, one obtains $\gamma = 6.95$ for $u\bar{u}$ and $d\bar{d}$ pair creation, and $\gamma = 6.95/\sqrt{3}$ for $s\bar{s}$ pair creation [72]. The flavor wave function of the quark-antiquark pair is given by $\phi_0 = (u\bar{u} + d\bar{d} + s\bar{s})/\sqrt{3}$, and the color wave function is $\omega_0 = (r\bar{r} + g\bar{g} + b\bar{b})/\sqrt{3}$. The operator in the model is

$$T = -3\gamma\sum_m \langle 1m1-m|00\rangle \int \mathrm{d}\mathbf{p}_3\mathrm{d}\mathbf{p}_4\delta^3(\mathbf{p}_3+\mathbf{p}_4) \times \mathcal{Y}_1^m\left(\frac{\mathbf{p}_3-\mathbf{p}_4}{2}\right)\chi_{1-m}^{34}\phi_0^{34}\omega_0^{34}b_3^\dagger(\mathbf{p}_3)d_4^\dagger(\mathbf{p}_4), \tag{22}$$

The S-matrix element for the process $A \to B + C$ is expressed as

$$\langle BC|T|A\rangle = \delta^3(\mathbf{P}_A - \mathbf{P}_B - \mathbf{P}_C)\mathcal{M}^{M_{J_A}M_{J_B}M_{J_C}}, \tag{23}$$

where $\mathbf{P}_B$ and $\mathbf{P}_C$ are the momenta of B and C mesons in the final state; they satisfy $\mathbf{P}_A = \mathbf{P}_B + \mathbf{P}_C = 0$ in the center-of-mass frame of meson A. $\mathcal{M}^{M_{J_A}M_{J_B}M_{J_C}}$ is the helicity amplitude of the process $A \to B + C$, which can be obtained as

$$\begin{aligned}\mathcal{M}^{M_{J_A}M_{J_B}M_{J_C}}(\mathbf{P}) = \gamma\sqrt{8E_AE_BE_C}\sum_{M_{L_A},M_{S_A},M_{L_B},M_{S_B},M_{L_C},M_{S_C},m} &\langle L_AM_{L_A}S_AM_{S_A}|J_AM_{J_A}\rangle\langle L_BM_{L_B}S_BM_{S_B}|J_BM_{J_B}\rangle \\ \times\langle L_CM_{L_C}S_CM_{S_C}|J_CM_{J_C}\rangle&\langle 1m1-m|00\rangle\langle\chi_{S_BM_{S_B}}^{14}\chi_{S_CM_{S_C}}^{32}|\chi_{S_AM_{S_A}}^{12}\chi_{1-m}^{34}\rangle[\langle\phi_B^{14}\phi_C^{32}|\phi_A^{12}\phi_0^{34}\rangle\mathcal{I}_{M_{L_B},M_{L_C}}^{M_{L_A},m}(\mathbf{P},m_1,m_2,m_3) \\ +(-1)^{1+S_A+S_B+S_C}&\langle\phi_B^{32}\phi_C^{14}|\phi_A^{12}\phi_0^{34}\rangle\mathcal{I}_{M_{L_B},M_{L_C}}^{M_{L_A},m}(-\mathbf{P},m_2,m_1,m_3)],\end{aligned} \tag{24}$$

with the momentum space integral

$$\mathcal{I}_{M_{L_B},M_{L_C}}^{M_{L_A},m}(\mathbf{P},m_1,m_2,m_3) = \int \mathrm{d}\mathbf{p}\,\psi_{n_BL_BM_{L_B}}^*\left(\frac{m_3}{m_1+m_3}\mathbf{P}+\mathbf{p}\right)\psi_{n_CL_CM_{L_C}}^*\left(\frac{m_3}{m_2+m_3}\mathbf{P}+\mathbf{p}\right)\psi_{n_AL_AM_{L_A}}(\mathbf{P}+\mathbf{p})\mathcal{Y}_1^m(\mathbf{p}), \tag{25}$$

where $\mathbf{P}=\mathbf{P}_B=-\mathbf{P}_C$, $\mathbf{p}=\mathbf{p}_3$, and m_3 is the mass of the created quark q_3. To analyze the results and compare the theoretical results with experimental data, the partial wave amplitude $\mathcal{M}^{JL}(A\to BC)$ is often employed. It is related with the helicity amplitude by the Jacob-Wick formula [73]:

$$\mathcal{M}^{JL}(A\to BC)=\frac{\sqrt{2L+1}}{2J_A+1}\sum_{M_{J_B},M_{J_C}}\langle L0JM_{J_A}|J_AM_{J_A}\rangle \times\langle J_BM_{J_B}J_CM_{J_C}|JM_{J_A}\rangle\mathcal{M}^{M_{J_A}M_{J_B}M_{J_C}}(\mathbf{P}). \tag{26}$$

Finally, the decay width is calculated as

$$\Gamma=\pi^2\frac{|\mathbf{P}|}{M_A^2}\sum_{JL}\left|\mathcal{M}^{JL}\right|^2, \tag{27}$$

where a nonrelativistic phase-space is assumed,

$$|\mathbf{P}|=\frac{\sqrt{[M_A^2-(M_B+M_C)^2][M_A^2-(M_B-M_C)^2]}}{2M_A}, \tag{28}$$

with M_A, M_B, M_C being the masses of the mesons involved. In this study, for computational convenience, we transformed the transition operator T from the momentum space to the coordinate space. The specific form is

$$T_2=-3\gamma\sum_m\langle 1m1-m|00\rangle\int \mathrm{d}\mathbf{r_3}\mathrm{d}\mathbf{r_4}(\frac{1}{2\pi})^{3/2}ir2^{-5/2}f^{-5} \times Y_{1m}(\hat{\mathbf{r}})\mathrm{e}^{-\frac{r^2}{4f^2}}\mathrm{e}^{-\frac{R_{AV}^2}{f_0^2}}\chi_{1-m}^{34}\phi_0^{34}\omega_0^{34}b_3^\dagger(\mathbf{r_3})d_4^\dagger(\mathbf{r_4}). \tag{29}$$

Here, $\mathbf{R}_{AV}=\mathbf{R}_A-\mathbf{R}_V$ is the relative coordinate between the source particle "A" and the created quark-antiquark pair in the vacuum, with

$$\mathbf{R}_A=\frac{m_1\mathbf{r_1}+m_2\mathbf{r_2}}{m_1+m_2};$$

$$\mathbf{R}_V=\frac{m_3\mathbf{r_3}+m_4\mathbf{r_4}}{m_3+m_4}=\frac{\mathbf{r_3}+\mathbf{r_4}}{2}.$$

The convergence factor $\mathrm{e}^{-r^2/(4f^2)}$ in the modified operator T_2 accounts primarily for energy considerations of the quark-antiquark pairs created in the vacuum, confirming the difficulty of creating high-energy quark-antiquark pairs. The damping factor $\mathrm{e}^{-R_{AV}^2/{R_0}^2}$ reflects that the created quark-antiquark pair should not be too far from the originating particle. Finally, the parameter $\gamma=6.95$ was initially obtained by fitting the heavy-flavor meson $c\bar{c}$. However, a previous study of ours demonstrated that this parameter cannot be directly applied to the calculation of mass shifts in the light meson spectrum [74]. In this context, we need to calculate the decay of the light meson K^*. Therefore, we first obtained a new value for γ by fitting the experimental data for $\rho\to\pi\pi$. The values of the parameters R_0 and f were ultimately determined by fitting the masses of light mesons,

$$\gamma=32.2,\quad f=0.5\ \text{fm},\quad R_0=1.0\ \text{fm}.$$

V. RESULTS AND DISCUSSION

We systematically studied the bound and resonant states in T_{ss}. We coupled the diquark and molecular structures to explore potential bound states, denoted as KK^*. Within the framework of the four-quark model, the KK^* states cannot decay via strong interactions into other two-meson channels. Therefore, the decay width of bound states KK^* can only originate from the process of $K^*\to K\pi$. Using the $^3P_0$ model, we first calculated the decay width of K^* in vacuum based on previously fitted parameters of light mesons. Then, we calculated the decay width of K^* when bound in the KK^* state, taking into account the effects of binding energy. By comparing these two results, we estimated the decay width of the bound state KK^*. Finally, we employed the real-scaling method to systematically identify resonant states in the energy range from 1.4 to 2.8 GeV and calculated their decay widths.

A. Bound-state calculation

Table 2 summarizes the results of the bound-state calculations. Owing to symmetry restrictions, the molecular structure of the T_{ss} system with 01^+ involves four physical channels: two color singlets, KK^* and K^*K^*, and their corresponding color octets. Meanwhile, the diquark structure of the T_{ss} system contains only two physical channels: $[ss]_6^0[\bar{q}\bar{q}]_{\bar{6}}^1$ and $[ss]_3^1[\bar{q}\bar{q}]_{\bar{3}}^0$.

The energy of KK^* is 1393 MeV, which is 1 MeV above the threshold (1392 MeV). Its color octet state, $[K]_8[K^*]_8$, has an energy of 1959 MeV, which is significantly higher than the threshold energy, indicating that neither of these channels form bound states. By contrast, K^*K^* has an energy of 1816 MeV, whereas its color octet state, $[K^*]_8[K^*]_8$, has an energy of 1797 MeV. This energy is not only lower than that of $[K]_8[K^*]_8$ but also lower than the energy of K^*K^*. This can be attributed to the fact that, within the quark model, strong attractive forces are more likely to occur between double vector mesons [75]. We performed channel coupling for these four molecular states. The results indicate that, although K^*K^* and $[K^*]_8[K^*]_8$ exhibit strong attractive interactions, the coupling effect still do not lower the energy of the lowest energy channel KK^* below the threshold. Simil-

Table 2. Results of the bound state calculations in the $s\bar{q}s\bar{q}$ system (unit: MeV).

Channel	$\|S_iF_jC_k\rangle(\Psi^{i,j,k})$	E	Mixed
KK^*	$\|111\rangle$	1393	
$[K]_8[K^*]_8$	$\|112\rangle$	1959	
K^*K^*	$\|311\rangle$	1816	
$[K^*]_8[K^*]_8$	$\|312\rangle$	1797	
coupled-molecular-channels:			1392
$[ss]^0_6[\bar{q}\bar{q}]^1_6$	$\|124\rangle$	1974	
$[ss]^1_3[\bar{q}\bar{q}]^0_{\bar{3}}$	$\|223\rangle$	1543	
coupled-diquark-channels:			1484
complete coupled-channels:			1328
Threshold (K+K^*):			1392

arly, owing to symmetry constraints, the diquark structure contains only two physical channels, $[ss]^0_6[\bar{q}\bar{q}]^1_6$ and $[ss]^1_3[\bar{q}\bar{q}]^0_{\bar{3}}$. Among these, the $3\times\bar{3}$ configuration has a relatively low energy of 1543 MeV, approximately 100 MeV above the threshold energy, whereas the $6\times\bar{6}$ configuration has a much higher energy and is heavier than all the molecular structures. This suggests that the diquark structure with $3\times\bar{3}$ exhibits stronger attraction. Subsequently, we performed structural mixing of the two physical channels in the diquark structure and the four physical channels in the molecular structure. The calculation results indicate that a bound state, $B(1320)$, with a binding energy of 60 MeV was obtained. The composition analysis reveals that the molecular state KK^* contributes 82% to $B(1320)$, while the $[ss]^1_3[\bar{q}\bar{q}]^0_{\bar{3}}$ state contributes 13%, as shown in Table 3. The root-mean-square distance of $B(1320)$ shows that the distance between internal quarks is approximately 1 fm, directly confirming that $B(1320)$ is predominantly a molecular state.

Similar to the decay width of T_{cc}, which mainly comes from $DD^*\to DD+\pi$, the decay width of the predicted bound state $B(1320)$ should mainly result from $KK^*\to KK+\pi$. T_{cc} has a binding energy of 1 MeV and hence only minimally affects the phase space for $DD^*\to DD+\pi$, resulting in a decay width almost equal to that of D^*. In contrast to T_{cc}, $B(1320)$ has a binding energy of 60 MeV, which substantially reduces the phase space for $KK^*\to KK+\pi$. As a result, the decay width of $B(1320)$ is expected to be less than that of K^*. To estimate the decay width of the bound state in the T_{ss} system (KK^*), we distributed the binding energy of 60 MeV equally between the two particles K and K^*. Consequently, the energy of K^* in KK^* had to be corrected by reducing it by approximately 30 MeV. The decay width of K^*, after this mass correction, provides the decay width of the bound state in the T_{ss} system (KK^*). Employing the $^3P_0$ model, we calculated the decay widths of K^* and K^* within the bound state KK^* separately. The results are listed in Table 4. We observed, that owing to the influence of the binding energy, the decay width of K^* decreased from 20 to 17 MeV. Therefore, we hypothesize that the width of the bound state $B(1320)$ we obtained should be approximately 3 MeV smaller than the experimentally observed width of K^*.

B. Resonant-state calculation:

In the quark model, resonances can form through two types of mechanism: the first involves strong attraction between mesons, resulting in resonance states, and the second involves resonance formation due to attractive interactions between colorful structures. Given that, in the T_{ss} bound state calculations, every single channel is a scattering state, the first mechanism does not apply. Thus, we focused on identifying resonances under the second mechanism framework.

In the T_{ss} system, there are four colorful structures: two diquark configurations, $[ss]^0_6[\bar{q}\bar{q}]^1_6$ and $[ss]^1_3[\bar{q}\bar{q}]^0_{\bar{3}}$, and two color-octet states, $[K]_8[K^*]_8$ and $[K^*]_8[K^*]_8$. We first performed channel coupling of these four colorful structures. According to our calculations, within the energy range of 1.4−2.8 GeV, we identified 13 possible candidates of resonance in the T_{ss} system. These resonances, denoted as E (energy), are listed in Table 5 along with their corresponding color structure compositions. The majority of the candidates are located around 2.6 GeV, indicating several genuine resonances at this energy level. Subsequently, we employed the real-scaling method to evaluate the stability of these resonances and obtained the results presented in Fig. 2. As shown in Fig. 2, most of the resonance candidates decayed into their corresponding threshold channels. Only four resonances, $R(2290)$, $R(2610)$, $R(2690)$, and $R(2740)$, survived the coupling process with the scattering channels. The resonance $R(2290)$ primarily originated from the previous resonance candidate $E(2313)$. As the scaling factor α increased, the calculational space changed, causing the energy of $E(2313)$ to drop to 2290 MeV, where it stabilized and formed an avoid-crossing structure at $\alpha=1.2$. The energies of most resonance candidates are concentrated around 2.6 GeV. Note that the other three genuine resonances that survive after coupling with the scattering chan-

Table 3. Main components of the bound state and root-mean-square distance among the internal quarks (unit: fm).

State	KK^*	$[ss]^1_3[\bar{q}\bar{q}]^0_{\bar{3}}$	K^*K^*	$[K^*]_8[K^*]_8$	$r_{s\bar{s}}$	$r_{s\bar{q}}$	$r_{\bar{q}\bar{q}}$
$B(1320)$	82%	13%	3%	2%	1.0	1.1	1.3

Table 4. Comparison of the calculated decay widths of K^* in vacuum and in the KK^* bound state.

State	$K\pi$	State	$K\pi$
K^*	20 MeV	K^* in the KK^*	17 MeV

Table 5. Candidates for resonant states in the $s\bar{q}s\bar{q}$ system (unit: MeV).

Resonances	$[ss]^0_6[\bar{q}\bar{q}]^1_6$	$[ss]^1_3[\bar{q}\bar{q}]^0_3$	$[K]_8[K^*]_8$	$[K^*]_8[K^*]_8$
$E(1484)$	8.7%	83.3%	1.1%	6.9%
$E(1875)$	68.2%	1.0%	12.8%	18.0%
$E(2099)$	12.0%	63.4%	5.6%	18.9%
$E(2229)$	1.3%	69.0%	18.6%	11.1%
$E(2313)$	68.3%	9.2%	8.4%	14.1%
$E(2345)$	0.9%	59.6%	21.1%	18.4%
$E(2541)$	17.0%	56.0%	15.3%	11.7%
$E(2618)$	34.9%	9.9%	31.5%	23.6%
$E(2631)$	2.9%	59.3%	25.5%	12.1%
$E(2669)$	18.4%	33.0%	8.2%	40.4%
$E(2681)$	4.3%	49.1%	42.2%	6.3%
$E(2726)$	45.5%	19.2%	11.4%	23.9%
$E(2751)$	1.4%	60.7%	18.3%	19.5%

nels also have energies near 2.6 GeV. By comparing the energy levels, we can infer that resonance $R(2620)$ likely originated from candidate $E(2618)$, resonance $R(2680)$ from candidate $E(2682)$, and resonance $R(2740)$ from candidate $E(2751)$. We also calculated the percentage contributions of each channel and the root-mean-square distance between quarks for these resonances, as listed in Table 6. This table shows that each resonance has a significant $[K^*]_8[K^*]_8$ component. From our previous bound state calculations, we already observed that the energy of $[K^*]_8[K^*]_8$ is lower than that of K^*K^*, indicating a strong attraction between $[K^*]_8[K^*]_8$. Given that these four resonances contain substantial colorful structure components, their internal quark distances are small, within 1 fm. Additionally, their decay widths are all less than 10 MeV.

VI. SUMMARY

In the framework of the chiral quark model, we systematically investigated the bound states and resonances of the T_{ss} ($s\bar{q}s\bar{q}$ with 01^+) system. Using the method of Gaussian expansion, we considered four physical channels, KK^* and K^*K^*, and their corresponding color octets, $[K]_8[K^*]_8$ and $[K^*]_8[K^*]_8$, in the molecular structure, as well as two physical channels, $[ss]^0_6[\bar{q}\bar{q}]^1_6$ and $[ss]^1_3[\bar{q}\bar{q}]^0_3$, in the diquark structure, and performed coupled-channel calculations for these two structures.

The bound state calculations reveal a deeply bound state, $B(1330)$, with KK^* as its primary component. We hypothesize that the main decay width of this bound state arises from the decay process $K^* \to K+\pi$. Thus, using the $^3P_0$ model, we calculated the decay width of K^* to be 20 MeV. However, the binding energy of $B(1330)$, approximately 60 MeV, directly affects the decay phase space of K^*. By distributing this binding energy equally between

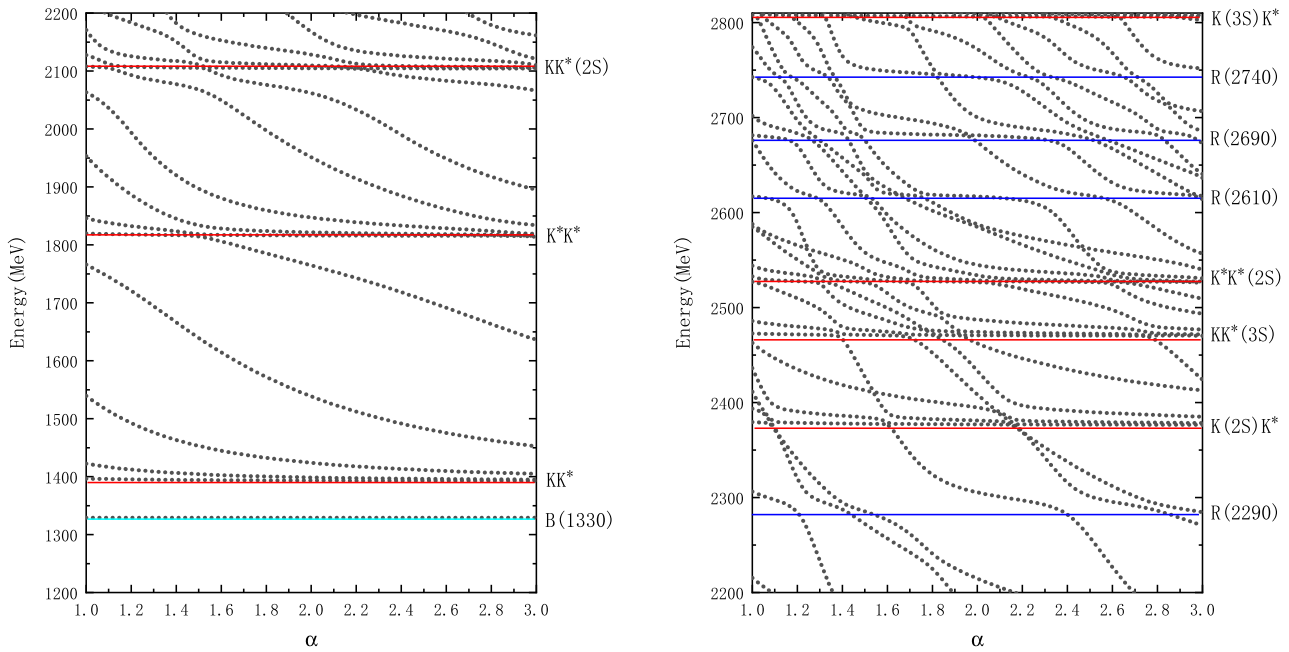

(a)Energy range from 1.2 GeV to 2.2 GeV (b)Energy range from 2.2 GeV to 2.8 GeV

Fig. 2. (color online) Energy spectrum of the T_{ss} system obtained from the real-scaling method.

Table 6. Decay widths of the resonance states, main components of the resonance states (unit: MeV), and root-mean-square distances (unit: fm) in the $ss\bar{q}\bar{q}$ system.

state	width	KK^*	$[K]_8[K^*]_8$	K^*K^*	$[K^*]_8[K^*]_8$	$[ss]^1_3[\bar{q}\bar{q}]^0_{\bar{3}}$	$[ss]^0_6[\bar{q}\bar{q}]^1_{\bar{6}}$	$r_{s\bar{s}}$	$r_{s\bar{q}}$	$r_{\bar{q}\bar{q}}$
$R(2290)$	10.2	17.2%	8.0%	9.8%	36.4%	5.8%	22.4%	1.1	1.2	1.4
$R(2620)$	5.3	19.6%	24.8%	0.9%	36.3%	15.0%	3.2%	1.2	1.4	1.5
$R(2680)$	5.8	5.4%	25.5%	15.1%	28.9%	7.3%	17.6%	1.2	1.3	1.4
$R(2740)$	1.9	7.4%	14.5%	1.6%	35.1%	0.3%	40.1%	0.9	1.0	1.2

K^* and K, we estimated that the energy of K^* should be reduced by approximately 30 MeV during the decay process. Consequently, the decay width of the bound state $B(1330)$ in the T_{ss} system is estimated to be 17 MeV. Subsequently, we employed the real-scaling method to calculate the resonances. These results indicate that we obtained four resonances, $R(2290)$, $R(2610)$, $R(2690)$, and $R(2740)$, primarily composed of colorful structure components. Their decay widths are all within 10 MeV, and the internal quark distances are around 1 fm.

Given the current interest in T_{cc}, with much attention focused on its heavy-flavor partner, there is limited research on the light-flavor partner of T_{cc}. Therefore, we suggest that related experiments must be conducted to search for the predicted bound states and resonances in the T_{ss} system.

References

[1] M. Gell-Mann, Phys. Lett. **8**, 214 (1964)
[2] G. Zweig, CERN-TH-412.
[3] S. K. Choi *et al.* (Belle), Phys. Rev. Lett. **91**, 262001 (2003)
[4] S. Jia *et al.* (Belle), Phys. Rev. D **100**, 111103 (2019)
[5] M. Ablikim *et al.* (BESIII), Phys. Rev. Lett. **110**, 252001 (2013)
[6] R. Aaij *et al.* (LHCb), Nature Commun. **13**, 3351 (2022)
[7] R. Aaij *et al.* (LHCb), Nature Phys. **18**, 751 (2022)
[8] M. L. Du, V. Baru, X. K. Dong *et al.*, Phys. Rev. D **105**, 014024 (2022)
[9] Y. Huang, H. Q. Zhu, L. S. Geng *et al.*, Phys. Rev. D **104**, 116008 (2021)
[10] S. S. Agaev, K. Azizi, and H. Sundu, Nucl. Phys. B **975**, 115650 (2022)
[11] E. Braaten, L. P. He, K. Ingles *et al.*, Phys. Rev. D **106**, 034033 (2022)
[12] N. N. Achasov and G. N. Shestakov, Phys. Rev. D **105**, 096038 (2022)
[13] N. Li, Z. F. Sun, X. Liu *et al.*, Phys. Rev. D **88**, 114008 (2013)
[14] J. B. Cheng, S. Y. Li, Y. R. Liu *et al.*, Chin. Phys. C **45**, 043102 (2021)
[15] Z. H. Lin, C. S. An, and C. R. Deng, Phys. Rev. D **109**, 056005 (2024)
[16] W. Chen, T. G. Steele, and S. L. Zhu, Phys. Rev. D **89**, 054037 (2014)
[17] Q. N. Wang and W. Chen, Eur. Phys. J. C **80**, 389 (2020)
[18] C. Deng and S. L. Zhu, Phys. Rev. D **105**, 054015 (2022)
[19] E. Braaten, L. P. He, and A. Mohapatra, Phys. Rev. D **103**, 016001 (2021)
[20] M. Karliner and J. L. Rosner, Phys. Rev. D **105**, 034020 (2022)
[21] S. Collins, A. Nefediev, M. Padmanath *et al.*, arXiv: 2402.14715[hep-lat]
[22] Y. Ikeda, B. Charron, S. Aoki *et al.*, Phys. Lett. B **729**, 85 (2014)
[23] P. Junnarkar, N. Mathur, and M. Padmanath, Phys. Rev. D **99**, 034507 (2019)
[24] J. B. Wang, G. Li, C. S. An *et al.*, Eur. Phys. J. C **82**, 721 (2022)
[25] Q. F. Lü, D. Y. Chen, and Y. B. Dong, Phys. Rev. D **102**, 034012 (2020)
[26] J. Vijande, A. Valcarce, and N. Barnea, Phys. Rev. D **79**, 074010 (2009)
[27] Q. Meng, E. Hiyama, A. Hosaka *et al.*, Phys. Lett. B **814**, 136095 (2021)
[28] D. Ebert, R. N. Faustov, V. O. Galkin *et al.*, Phys. Rev. D **76**, 114015 (2007)
[29] Y. Tan, W. Lu, and J. Ping, Eur. Phys. J. Plus **135**, 716 (2020)
[30] Y. Tan, X. Liu, X. Chen *et al.*, Phys. Rev. D **109**(7), 076026 (2024)
[31] Y. Yang, C. Deng, J. Ping *et al.*, Phys. Rev. D **80**, 114023 (2009)
[32] S. S. Agaev, K. Azizi, and H. Sundu, JHEP **06**, 057 (2022)
[33] F. S. Navarra, M. Nielsen, and S. H. Lee, Phys. Lett. B **649**, 166 (2007)
[34] A. Feijoo, W. H. Liang, and E. Oset, Phys. Rev. D **104**, 114015 (2021)
[35] L. Meng, G. J. Wang, B. Wang *et al.*, Phys. Rev. D **104**, L051502 (2021)
[36] R. Chen, Q. Huang, X. Liu *et al.*, Phys. Rev. D **104**, 114042 (2021)
[37] M. J. Yan and M. P. Valderrama, Phys. Rev. D **105**, 014007 (2022)
[38] X. K. Dong, F. K. Guo, and B. S. Zou, Commun. Theor. Phys. **73**, 125201 (2021)
[39] S. Fleming, R. Hodges, and T. Mehen, Phys. Rev. D **104**, 116010 (2021)
[40] Y. Hu, J. Liao, E. Wang, Q. Wang *et al.*, Phys. Rev. D **104**, L111502 (2021)
[41] K. Chen, R. Chen, L. Meng *et al.*, Eur. Phys. J. C **82**, 581 (2022)
[42] B. Wang and L. Meng, Phys. Rev. D **107**, 094002 (2023)
[43] X. Z. Ling, M. Z. Liu, L. S. Geng *et al.*, Phys. Lett. B **826**, 136897 (2022)
[44] H. W. Ke, X. H. Liu, and X. Q. Li, Eur. Phys. J. C **82**, 144

(2022)
[45] J. He and X. Liu, Eur. Phys. J. C **82**, 387 (2022)
[46] L. M. Abreu, H. P. L. Vieira, and F. S. Navarra, Phys. Rev. D **105**, 116029 (2022)
[47] K. Azizi and U. Özdem, Phys. Rev. D **104**, 114002 (2021)
[48] Y. Lyu, S. Aoki, T. Doi *et al.*, Phys. Rev. Lett. **131**, 161901 (2023)
[49] Y. Kim, M. Oka, and K. Suzuki, Phys. Rev. D **105**, 074021 (2022)
[50] Q. Meng, M. Harada, E. Hiyama *et al.*, Phys. Lett. B **824**, 136800 (2022)
[51] R. Albuquerque, S. Narison, and D. Rabetiarivony, Nucl. Phys. A **1034**, 122637 (2023)
[52] S. S. Agaev, K. Azizi, B. Barsbay, and H. Sundu, Phys. Rev. D **101**, 094026 (2020)
[53] E. Hernández, J. Vijande, A. Valcarce *et al.*, Phys. Lett. B **800**, 135073 (2020)
[54] J. Carlson, L. Heller, and J. A. Tjon, Phys. Rev. D **37**, 744 (1988)
[55] S. Pepin, F. Stancu, M. Genovese *et al.*, Phys. Lett. B **393**, 119 (1997)
[56] M. Pflaumer, L. Leskovec, S. Meinel *et al.*, PoS LATTICE **2021**, 392 (2022)
[57] T. Guo, J. Li, J. Zhao, and L. He, Phys. Rev. D **105**, 014021 (2022)
[58] X. Z. Weng, W. Z. Deng, and S. L. Zhu, Chin. Phys. C **46**, 013102 (2022)
[59] L. R. Dai, R. Molina, and E. Oset, Phys. Rev. D **105**, 016029 (2022)
[60] Y. C. Yang, Z. Y. Tan, J. Ping *et al.*, Eur. Phys. J. C **77**(9), 575 (2017)
[61] Y. Tan, X. Liu, X. Chen *et al.*, arXiv: 2404.02048[hep-ph]
[62] J. Vijande, F. Fernandez, and A. Valcarce, J. Phys. G **31**, 481 (2005)
[63] H.S. Taylor, Models, Advan. Chem. Phys. **18**, 91 (1970)
[64] E. Hiyama, A. Hosaka, M. Oka *et al.*, Phys. Rev. C **98**, 045208 (2018)
[65] Y. Tan and J. Ping, Phys. Rev. D **101**, 054010 (2020)
[66] Y. Tan and J. Ping, Chin. Phys. C **45**, 093104 (2021)
[67] Y. Tan, X. Liu, X. Chen *et al.*, Phys. Rev. D **108**, 014017 (2023)
[68] Y. Tan, Y. Wu, H. Huang *et al.*, Universe **10**, 17 (2024)
[69] Y. Wu, Y. Yan, Y. Tan *et al.*, Phys. Rev. D **109**, 096005 (2024)
[70] L. Micu, Nucl. Phys. B **10**, 521 (1969)
[71] A. Le Yaouanc, L. Oliver, O. Pene *et al.*, Phys. Rev. D **8**, 2223 (1973)
[72] A. Le Yaouanc, L. Oliver, O. Pene *et al.*, Phys. Lett. B **72**, 57 (1977)
[73] M. Jacob and G. C. Wick, Annals Phys. **7**, 404 (1959)
[74] X. Chen, J. Ping, C. D. Roberts *et al.*, Phys. Rev. D **97**(9), 094016 (2018)
[75] Y. Wu, X. Jin, H. Huang *et al.*, Phys. Rev. C **106**, 025204 (2022)